Photoelectron imaging spectroscopy of small tungsten clusters: Direct observation of thermionic emission

B. Baguenard, J. C. Pinaré, C. Bordas, and M. Broyer
Laboratoire de Spectrométrie Ionique et Moléculaire, 43 Boulevard du 11 Novembre 1918, F69622 Villeurbanne Cedex, France
(Received 2 August 2000; published 16 January 2001)

Single-photon photodetachment of mass-selected W_n^- clusters has been studied by photoelectron imaging spectroscopy. Velocity map imaging allows us to measure simultaneously the kinetic-energy spectrum and the angular distribution of photoelectrons. This provides a clear distinction between the two major decay mechanisms: isotropic thermionic emission and anisotropic direct photoemission. A careful study of threshold electrons shows that the thermal distribution cannot be described by a bulklike formula or a simple exponentially decreasing Boltzmann function. On the contrary, our results are in excellent agreement with more refined theoretical models taking into account the spherical symmetry of the cluster. The kinetic-energy distribution of thermal electrons corresponding to thermionic emission is found to vary as $p(\epsilon) \propto \epsilon^{1/2} \exp(-\epsilon/k_B T)$. Our results indicate that a transition toward a bulklike statistical behavior of the internal-energy redistribution occurs in very small systems owing to the high density of states in metal clusters. Moreover, the angular distribution of direct photoelectrons is obtained and the evolution as a function of size is discussed. The asymmetry parameter β of the most intense band observed in direct photoemission for each cluster decreases monotonically with size: the direct photoemission of smaller systems is strongly anisotropic, becoming isotropic as the size of the system increases. This probably indicates the loss of coherence induced by electron-electron collisions occurring in large systems.

DOI: 10.1103/PhysRevA.63.023204 PACS number(s): 36.40.−c, 33.60.Cv

I. INTRODUCTION

The time evolution of complex microscopic systems is essentially governed by the nonadiabatic couplings between the various electronic and nuclear degrees of freedom. Investigating the internal dynamics of such systems has become one of the most active fields in molecular and cluster physics. Various experimental techniques may be used to access the internal dynamics. Schematically, two kinds of experiment may be distinguished. First, the time evolution may be probed directly. Pump-probe ultrafast laser spectroscopy allows in many cases a remarkable insight into the details of the nonadiabatic couplings involved in the system. Analysis of the kinematics of the ejected particles (fragments, electrons, photons, etc.) is a different route to access the internal dynamics. In this second category of experiments, the energy and spatial distributions together with branching ratios are measured without direct access to time-dependent variables. The work presented in this paper pertains to this family of experiments.

Indeed, it is of primary importance to understand the evolution of a microscopic system after the absorption of a single photon, because it is the prototype of a physical problem where one has total control of the quantity of energy deposited in the system together with a limited number of internal conversion processes. The optical excitation of an isolated molecule or cluster by absorption of a single photon results in a decay process that follows different channels (emission of atoms, molecules, electrons, or photons) according to the size of the particle, its internal energy, and the relative values of the barriers relevant to the various decay paths. From this point of view, metallic or covalent clusters consisting of a few to many hundreds of atoms of a single element are among the simplest models for studying the dynamics of complex systems containing an arbitrarily large number of degrees of freedom.

The work presented here deals with a specific and fundamental aspect of this problem, namely, what is the behavior of energy-rich clusters where the excitation energy exceeds the threshold required for the emission of an electron. Fragmentation processes are not examined here since only refractory compounds are studied. This includes excitation above the ionization threshold in the case of neutral species, or above the detachment threshold in the case of anions. Clusters excited in the ionization or detachment continuum provide a physical regime where a complete breakdown of the Born-Oppenheimer approximation is likely to occur. From this point of view, the analogy with the field of molecular Rydberg states and autoionization is striking. Electron-nucleus couplings are determinant and the dynamics of the system is governed by the exchange of energy between the electronic and vibronic degrees of freedom. The consequence of these couplings is that the emission of electrons is not simply governed by the energy (which allows or forbids the process itself) but also by the strength of the various couplings, with the result that the electron does not carry away all the residual energy and may take a long time before being ejected. This is at the origin of the distinction between prompt and delayed emission [1–5]. Delayed ionization [5] has been observed mainly from metal [6–11] or carbon [12–14] clusters, but also from large molecules [1,2] where internal-energy conversion is a common process. Delayed ionization corresponds typically to electron emission occurring in the range of tens of nanoseconds up to many micro- or even milliseconds after excitation. When the internal-energy redistribution presents a statistical character, this phenomenon is described as thermionic emission, by analogy

with the emission of electrons from hot bulk material. This is particularly true when observed from clusters which, to some extent, behave like a small piece of bulk material. The term of thermionic emission implies that the excitation energy is equipartitioned between the nuclear and electronic degrees of freedom. However, electron emission is not necessarily the only decay channel and the competition with evaporation of atoms or molecules, fragmentation, and radiative cooling must be taken into account. The work presented here is limited to the situation where electron emission is, by far, the dominant channel. This is the general rule in refractory systems such as small negative tungsten clusters where the electron affinity is noticeably smaller than the dissociation energy. However, the situation is much more complex in general owing to the relative values of the barriers to the emission of electrons or atoms, which are often comparable in neutral clusters. Nevertheless, a detailed understanding of such phenomena in the case where a single decay channel may be isolated allows us to probe more precisely the fundamental dynamical processes that occur in energy-rich clusters.

Delayed ionization occurring in a time domain ranging from a few microseconds to several milliseconds after laser excitation was first reported in neutral metal clusters [7–11,15,16] and in fullerenes [12–14,17–30]. Tungsten clusters have received special attention [31–33]. After this preliminary work, much effort has been concentrated on negative clusters (metal [6,34–39] and carbon [40–42]), where delayed ionization may occur at a shorter time scale and with a higher rate. By analogy with condensed matter physics [43], this delayed ionization has been designated ''thermionic emission.'' This implies that a free cluster excited above threshold samples all the phase space available before electron emission. In order to assume this equilibrium, electron-phonon couplings have to be fast with respect to the rate of ionization or detachment. This is often the case with a typical time scale of a few picoseconds for internal conversion. Under this condition, the ionization/detachment rate can be equated with the rate at equilibrium. However, it is not completely clear at the present time that this is the general case since experimentally measured thermionic emission rates are often several orders of magnitude smaller than expected. This suggests that the rate of internal conversion may be more determining than the emission rate itself in the overall decay rate. This was emphasized by Remacle and Levine [3], who consider that the decay rate is mostly determined by the energy exchange between electrons and vibrations in electronically excited molecules or clusters. In such cases the decay rate is limited by the existence of internal bottlenecks. Such effects have been evidenced, for example, in resonant infrared multiphoton ionization of fullerenes using a free-electron laser [44,45].

In the work presented here, we do not focus on the internal process itself or on the precise determination of decay rates. Rather, we try to examine carefully the kinetic-energy distribution of slow photoelectrons, which is one of the most direct probes to confirm whether or not thermal equilibrium is reached prior to delayed ionization. Indeed, the kinetic-energy distribution of photoelectrons provides valuable information on the ionization mechanism. Some authors have used a simple Boltzmann distribution to fit their experimental data [34,35]. This is absolutely not justified in a negatively charged finite-size system with spherical symmetry. A quantitative comparison of our experimental energy distribution with the most sophisticated model of thermionic emission in finite-size systems derived by Klots [46–53] will allow us to confirm this character in small refractory clusters. This quantitative comparison has been made possible by the use of the velocity map imaging technique [54,55], which is particularly well suited to determining slow-photoelectron kinetic-energy distributions. The constant sensitivity of the method, especially near threshold, allows extraction of reliable threshold laws from experimental data that provides a stringent test of the theoretical models and a sensitive comparison of the different means of excitation.

II. SUMMARY OF THE DECAY MECHANISMS

The key parameters that govern the evolution of the system are on one side the different barriers relative to the emission of the different particles, and on the other side the internal couplings that drive the system toward the various open final channels. It is a common approximation to consider that the absorption of a single photon leads, in a first step, to the excitation of a single electron. Of course, this is an extremely simplistic assumption that is a strict application of the Born-Oppenheimer approximation and, depending on the overlap between initial and final wave functions of the system, it is clear that the initial optical excitation step leads to a non-negligible rovibrational excitation. At this point, we will describe the simplest scheme where all the photon energy is transferred to the external electron. After this first, instantaneous step, one can distinguish schematically between two different kinds of processes: on one hand, direct processes in which the system decays directly after the electronic excitation and, on the other hand, indirect processes where the electron can transfer part of its energy to the nuclei before decay. Besides the distribution of the internal energy over different modes, the major difference is that the time scales at which both kinds of processes occur are extremely different. Electronic time scales are on the order of 100 fs [56], while electron-vibration couplings may extend from the pico- to the millisecond range. At this point the statistical distribution of the energy, i.e., the thermalization of the system, is not assumed. However, in metal clusters where the couplings between the various modes are extremely efficient, it may be expected that a statistical distribution of the energy is reached at very small size. In that case, when the energy is equipartitioned over the different modes, the system heats up to a temperature T_i which depends on its internal energy U, the sum of its initial energy U_0 (initial temperature T_0) and the photon energy $h\nu$, and on its heat capacity $C_v(T)$. In the limit of the Dulong-Petit law [43] for a bulk metal containing N atoms, the heat capacity $C_v(T)$ is a constant, $C_v(T) = 3Nk_B$ (with k_B the Boltzmann constant). In this limit the internal temperature T_i may be written as

$$T_i = T_0 + \frac{h\nu}{3Nk_B}. \quad (1)$$

If N is small as in clusters, and in the limit of the microcanonical ensemble, which is strictly the situation here (the same internal energy for an ensemble of identical particles), this equation must be rewritten to take into account the expression for $C_v(T)$, which may be approximated by $(3N-7)k_B$. This expression assumes that the harmonic-oscillator approximation holds true for small clusters. Although not true in general, it seems fairly reasonable in tungsten clusters since the dissociation energy is extremely high (typically 7 eV) and a total amount of internal energy of 4 eV shared by $(3N-7)$ modes leaves the system in the harmonic regime. Under this assumption, the internal temperature of the clusters may be written as

$$T_i = T_0 + \frac{h\nu}{(3N-7)k_B}. \quad (2)$$

Note that, immediately after optical excitation and before complete thermalization of the system by electron-phonon couplings on a picosecond time scale, electron-electron couplings lead to an extremely high electronic temperature. This process is typically in the 10–100 fs range. However, complete thermalization is fast enough [56] to avoid the emission of very hot electrons, as opposed to recent experiments performed with ultrashort laser pulses [57]. After thermalization, the cluster may decay by emitting an electron, a photon, or a heavy particle (atom or molecule) according to the presence of various open channels. Schematically, the indirect decay channels corresponding to the emission of an electron, a photon, or an atom are, respectively, thermionic emission, blackbody radiation [58–61], and evaporation [62–65]. Besides the competition between these indirect decay channels, the competition with the direct channels (respectively, direct photoemission, radiative decay, and dissociation) must be considered. The branching among these various decay paths is governed (1) by the internal dynamics of the system and (2) by the relative values of the various emission thresholds with respect to the total energy of the system. In this article, we will focus on the case of refractory systems where direct dissociation or evaporation of an atom (or molecule) is negligible because not energetically possible. In this kind of system, the decay processes following heating of the cluster are emission of electrons (thermionic emission) or emission of photons (blackbody radiation). Note that indirect decays lead to a totally isotropic emission since the coherence of the excitation step is lost during the internal-energy redistribution process. On the other hand, in direct processes, coherence effects lead to an anisotropic emission of particles. At this point, the question is how a hot refractory cluster will decay: is it by emitting a photon or by emitting an electron? In fact, the decay paths followed by the system depend critically on the binding energy of the outer electron. In bulk matter, thermionic emission corresponds to the emission of electrons from a hot surface at temperature T according to a kinetic-energy distribution

$$p(\epsilon) \propto \epsilon \exp(-\epsilon/k_B T), \quad (3)$$

which presents a maximum at $\epsilon = k_B T$.

The kinetic-energy distribution is not merely the tail of the Fermi-Dirac energy distribution, which would lead to a simple exponential function. Indeed, in order to be ejected from the bulk, not only must the electron have a positive energy but also the component of its momentum perpendicular to the surface must exceed the Fermi momentum. Since the Fermi energy is larger by far than the excess energy, this severely restricts the angle of emission and introduces a term proportional to the kinetic energy ϵ in the expression for $p(\epsilon)$.

For an ideal surface, the total emission current is given by the Richardson-Dushman equation [43]:

$$J_{\mathrm{TE}} = \frac{4\pi m e k_B^2}{h^3} A T^2 \exp\left(\frac{-W}{k_B T}\right), \quad (4)$$

where W is the barrier to the emission of an electron, i.e., the work function in the case of bulk matter. A is a constant that depends on the material itself.

The power emitted by unit surface is

$$P \propto T^3 \exp\left(\frac{-W}{k_B T}\right). \quad (5)$$

The key point in the Richardson-Dushman formula is that the energy dissipated by electron emission is proportional to an exponential term that decreases very rapidly as the work function increases. Hence, no matter how fast the other decay channels are, the thermionic emission rate will be high in materials with low electron binding energy. On the other hand, blackbody radiation does not depend on electronic properties. In bulk matter, the energy dissipated by radiative cooling per unit of time is simply proportional to T^4:

$$P = \sigma T^4 = \frac{2\pi^5}{15} \frac{k_B^4}{c^2 h^3} T^4. \quad (6)$$

Let us now assume for the sake of simplicity that the emission rates are given qualitatively by similar relations for clusters. Then, in the case of tungsten, for example, one can use these equations in order to compare the various decay rates in bulk matter and in negative clusters. The bulk work function is about 4.5 eV, while the electron affinity of small negative tungsten clusters is about 1.5 eV. Replacing the bulk work function by the cluster electron affinity in Eq. (4) increases the emission rate by several orders of magnitude, especially at moderate temperature, while the blackbody rate is weakly affected. In addition, the dissociation energy in small negative tungsten clusters W_n^- $(n<15)$ (the bulk heat of vaporization) is on the order of 7 eV (8.9 eV) so that negative tungsten clusters are the prototypes of refractory systems and the best candidates to study thermionic emission in finite-size systems. As compared to fullerenes, for example, the situation is clearly simpler in tungsten cluster anions since the competition with other indirect processes is almost negligible. In the case presented here, the absorption

of a single visible or UV photon of energy $h\nu$ is sufficient to remove an electron from a finite-size negatively charged system [$h\nu$ is greater than the electron affinity (EA)]. The internal energy of the system in the photodetachment of W_n^- clusters by single-photon excitation is perfectly controlled. It is thus assumed that hot refractory cluster anions excited above the detachment threshold, and far below the dissociation threshold, may decay only by electronic emission. Thermionic emission (hereafter TE) is, to a very good approximation, only in competition with direct photoemission (hereafter DPE) where the excess energy is converted to photoelectron kinetic energy $\epsilon = h\nu - E_f$ (E_f is the energy of the final state of the target).

Photoelectron imaging spectroscopy [38,54,55,66–68] provides a very convenient way to distinguish between TE and DPE. In DPE, the features in the kinetic-energy photoelectron spectrum mirror the target excited-state spectrum: they are structured both in energy and in angular distribution. On the other hand, TE, as in the bulk and as described below, corresponds to a broad and isotropic distribution of slow electrons. In experimental images, the signal corresponding to thermionic emission will then lead to a centrally symmetric and smooth distribution surrounded by other, more structured, features corresponding to DPE at higher energy.

The bulklike functions Eqs. (3) and (4) describing both the energy distribution and the total emission rate are not relevant to finite-size systems. In finite-size species, the different symmetry of the system and the nature of the long-range interaction between the target and the ejected electron sensibly modify the energy distribution. Klots and coworkers [46–53] have extensively studied the detailed theoretical aspects of TE of spherical metallic clusters. These studies show that the kinetic-energy distribution $p(\epsilon)$ of thermal electrons in the limit of small-size particles is qualitatively different for negative systems where the long-range interaction between the final neutral target and the ejected electron is dominated by polarization terms, and neutral or positive systems where the long-range interaction is purely Coulombic. Moreover, owing to the finite size of the system, one has to distinguish between the internal temperature of the system T_i, given approximately by Eq. (2), and the emission temperature T_e. The emission temperature includes the finite-heat-bath correction [46–53]. A simple derivation of T_e may be found in [69]. Considering the energy barrier to electron emission (the electron affinity A_e in the case of anions), the emission temperature T_e may be written as (to first order in A_e/C_v)

$$T_e \approx T_i - \frac{A_e}{2C_v} \approx T_0 + \frac{h\nu - (A_e/2)}{(3N-7)k_B}. \tag{7}$$

From a qualitative point of view, the emission temperature T_e is the average of the internal microcanonical temperature T_i and the final temperature of the system after electron emission.

According to [46–53], the kinetic-energy distribution of TE of a cluster of N atoms of radius R_N ($R_N = r_s N^{1/3}$ with r_s the Wigner-Seitz radius) may be expressed as

$$p(\epsilon) \propto \{1 - \exp[-BL^2_{\max}(\epsilon)/k_B T_e]\} \exp(-\epsilon/k_B T_e). \tag{8}$$

Depending on the nature of the interaction between the escaping electron and the cluster, the maximum value of the angular momentum $L_{\max}$ of the outgoing electron may be written for a negatively charged system (only the polarization long-range potential) as

$$L^2_{\max}(\epsilon) = \left(\frac{2\mu}{\hbar^2}\right)[(2\alpha e^2 \epsilon)^{1/2} + \epsilon R_N^2 + \cdots] \tag{9}$$

and for a neutral or positively charged system (Coulomb long-range potential) as

$$L^2_{\max}(\epsilon) = \left(\frac{2\mu}{\hbar^2}\right)[e^2 R_N + \epsilon R_N^2 + \cdots], \tag{10}$$

with μ and e respectively the mass and charge of the electron, and α the static polarizability of the cluster. Because of the low mass of the electron, Eq. (8) may be rewritten as

$$p(\epsilon) \propto L^2_{\max}(\epsilon) \exp(-\epsilon/k_B T_e). \tag{11}$$

The most important difference between detachment and ionization arises from the expression of the maximum angular momentum of the outgoing electron $L_{\max}$ which is entirely determined by the asymptotic form of the potential. In the limit of small-size particles ($R_N \to 0$) the kinetic-energy distribution of thermionic emission may be approximated in photodetachment (anion) as

$$p(\epsilon) \propto \epsilon^{1/2} \exp(-\epsilon/k_B T_e), \tag{12}$$

and in photoionization (neutral or cation) as

$$p(\epsilon) \propto \exp(-\epsilon/k_B T_e). \tag{13}$$

Note that $p(\epsilon)$ vanishes for $\epsilon = 0$ in photodetachment while it remains finite in photoionization. For a given emission temperature T_e, the maximum of $p(\epsilon)$ is found at $\epsilon_0 = k_B T_e/2$ in photodetachment of a small negative cluster while $p(\epsilon)$ is maximum at $\epsilon_0 = k_B T_e$ in bulk (see Fig. 1). Finally, note also that $(k_B T_e/2)$ is only 0.1 eV at 2500 K so that standard photoelectron techniques are not appropriate for measuring such distributions since their sensitivity vanishes in that range.

The above discussion implies that the low-energy features in the spectrum correspond to indirect processes, and conversely that high-energy ones correspond to direct emission. This is certainly a schematic view, although it will be shown below that thermionic emission accounts for most of the electron signal at low energy. Moreover, assuming that all the excitation energy is transferred to the outer electron is an oversimplification and the details of the excitation and internal-conversion processes are more subtle. In particular, in the initial excitation step, the Born-Oppenheimer approximation does not hold and a large fraction of the photon energy may be converted immediately into vibrational excitation. Therefore, thermionic emission corresponds, at least partly, to vibrational autodetachment, and may not be attrib-

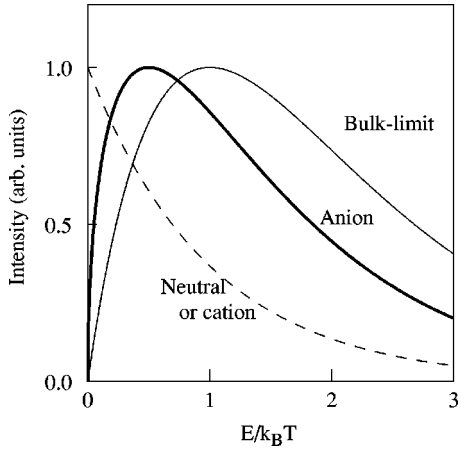

FIG. 1. Theoretical profiles of thermionic emission at a given temperature T in the bulk limit (thin solid line); in a small negative cluster (bold solid line); and in the case of a neutral or positive cluster (dashed line).

uted solely to internal-conversion processes. The discussion of the details of vibrational autodetachment and couplings is beyond the scope of this article. Nevertheless, the comparison of the experimental results with the model in Sec. IV will support the assumptions made here.

III. EXPERIMENTAL SETUP

Tungsten negative clusters are produced in a standard laser vaporization source [70]. The main difference between our experimental setup and other photoelectron spectroscopy experiments dealing with tungsten cluster anions [6,34–37] consists in our imaging spectrometer. Since the decay processes that we want to study are characterized by the emission of slow photoelectrons, we have chosen an experimental technique that allows the observation of threshold electrons with a constant efficiency over the whole range of energy. We use a recent evolution of the photoelectron imaging spectroscopy [66–68], namely, velocity map imaging [54,55]. Our experimental setup, schematized in Fig. 2, is briefly as follows. Negatively charged clusters are produced in a Milani–De Heer [71] type laser vaporization source seeded with helium. A 3-mm-diameter tungsten rod is vaporized with the second harmonic of a Nd:YAG (yttrium aluminum garnet) laser (or the fundamental of a Q-switched Ti:sapphire laser) at a repetition rate of 10 Hz. The helium carrier gas is injected at 5 bar via a solenoid pulsed valve. A key parameter for the study of thermal effects of clusters is the initial temperature of the clusters. In the present experiments, no particular cooling process has been used except the natural cooling of the adiabatic expansion. The temperature of the clusters is thus not perfectly controlled. This is not critical in the case of small clusters (as is the case here) because the absorption of a single photon brings the system to a very high temperature as compared to the initial temperature. However, this would be more relevant in the case of large clusters where a given temperature corresponds to a larger amount of internal energy. Under these conditions, the initial temperature of the clusters is close to room temperature and

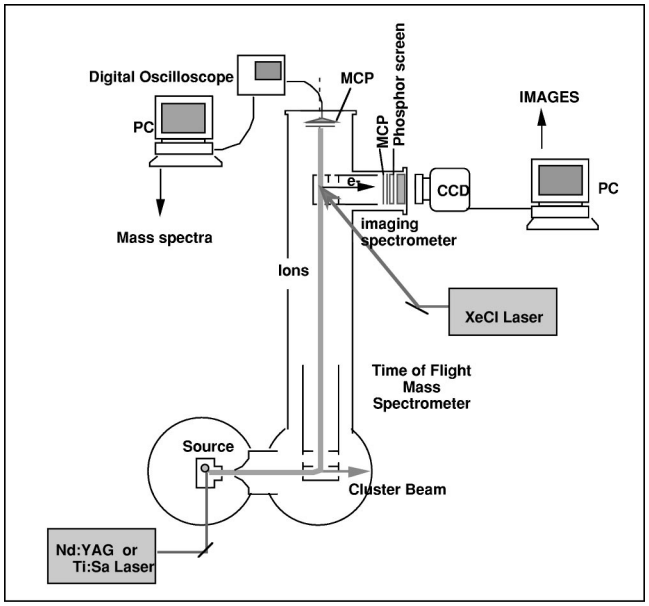

FIG. 2. Schematic of the experimental setup.

the initial temperature T_0 will be set to 300 K in further estimations. The laser vaporization source produces a large amount of neutral and positive clusters, and a smaller quantity of negative ions, especially at small size. This is due to the low electron affinity of small metal clusters. Attempts to increase the rate of production of small negative clusters by slow-electron bombardment have not been very successful yet. Native anions are extracted from the cluster beam in the extraction region of a Wiley-McLaren time-of-flight mass spectrometer (TOFMS) by a pulsed electric field. A pulse of about 3.5 kV is applied in the extraction region. The photoelectron spectrometer is located at the end of the TOFMS drift tube. As a consequence, the cluster anions arrive in separated bunches in the spectrometer according to their masses. No retardation field is applied in order to slow down the clusters before laser excitation in the electron spectrometer. In fact, the velocity dispersion of the cluster beam is completely negligible with respect to electron velocity in the spectrometer. The initial ''drift'' velocity of the electrons has the effect only of shifting the whole image by a negligible amount (at worst a few pixels) proportional to the cluster velocity. The excitation of a given cluster size is ensured by a proper delay between the pulsed extraction and the firing of the photodetachment laser. In the experiments described below we use a XeCl excimer laser ($\lambda = 308$ nm) for detachment.

The principle of the photoelectron imaging spectrometer is extremely simple [68]. A static electric field is applied in the photoelectron spectrometer to project the photoelectrons onto a position-sensitive detector. This results in an image that is the superposition of circular rings of radius proportional to the initial velocity with a filling pattern that reveals the original angular distribution with respect to the laser polarization. The distance between the impact of each electron on the position-sensitive detector and the center of the image is directly proportional to the projection of its initial velocity on the detector plane. The position-sensitive detector (PSD)

is made up of tandem microchannel plates (MCP's) followed by a phosphor screen (42 mm effective diameter). Each electron hitting the front MCP is converted to 10^6-10^7 photons. The photon signal is subsequently captured by a charge-coupled device (CCD) camera. We use a low-noise digital cooled CCD camera of 512×512 pixel resolution. Full detector area corresponds to 80–100 μm/pixel, which is optimal taking into account the resolution of the CCD/phosphor screen itself and the intrinsic spot size in the imaging spectrometer. After inversion [68], the image gives the initial energy and angular distribution of the photoelectrons.

The simplest scheme of imaging uses a homogeneous electric field for projecting the electrons onto the detector. This technique suffers from a major limitation, which is extremely restrictive in the present case. Indeed, the initial dispersion in the interaction region between the cluster and laser beams is preserved in this kind of projection and the smallest resolvable structure is at least of the size of the interaction region. This implies that the interaction region must be kept as small as possible in order to get a correct resolution. On the other hand, the cluster anion beam density is very low and the large dispersion of kinetic energy of the clusters due to the initial dispersion in the extraction region does not allow us to focus the ion beam correctly in the interaction region. Typically, an interaction region of about 2 mm diameter is required in order to obtain a significant signal. Since the effective area of the PSD is about 40 mm, this is totally unacceptable because it would limit the resolution of our device to less than $\frac{1}{10}$ in velocity. A minor modification of the experimental setup allows us to overcome this limitation. Parker and Eppink [54,55] recently introduced a very simple evolution of the imaging spectrometer where an inhomogeneous field generated by a set of three electrodes replaces the homogeneous field. A correct design allows compensating for the initial dispersion in position, while preserving the dispersion in initial velocity. The so-called ''velocity map imaging'' allows mapping of all electrons with the same initial velocity irrespective of their initial position, at least for a limited region around the center of the spectrometer. This modification allows working with a relatively large cluster beam/laser interaction zone, typically 2 mm in diameter, without degrading the image resolution. The final geometrical resolution on the detector is about 100–200 μm, i.e., 2 or 3 pixels on the CCD detector. In standard photoelectron spectroscopy techniques such as the magnetic bottle spectrometer [72], the measured quantity is the time of flight of the electron over a given distance. The consequence is that a slow-electron signal is spread over a large time range and moreover slow-photoelectron collection and detection efficiency vanishes below 0.1–0.2 eV. In contrast, in imaging spectroscopy, one directly measures the projection of the initial velocity of the ejected electron. Whatever the initial kinetic energy, the final kinetic energy is almost the same. This means that no slow electrons are lost between the source and the detector and the collection and detection efficiency is constant and independent of W. Also, the experimental velocity resolution is constant and equals δ/R, where δ is the experimental resolution (in pixels) and R the maximum radius image (in pixels). We have at the best $\delta=2$ while R is typically about 200, that is to say, a maximum resolution of $\frac{1}{100}$ in velocity. This resolution may be obtained under the most favorable experimental conditions and is not always achievable. From this point of view, imaging spectroscopy is not as good as the magnetic bottle, which offers a resolution of about 10 meV in the range 1–5 eV. This restriction is inherent in PSD techniques which are limited by geometrical constraints (number of pixels) while measurements of time of flight may be achieved with extremely high accuracy. However, at threshold, imaging is much more appropriate than standard techniques. Besides the fact that the detection efficiency does not vanish at zero energy, a resolution of $\frac{1}{100}$ in velocity at 200 meV corresponds to a resolution of 4 meV in energy. Provided that the signal-to-noise ratio is sufficient, meV resolution is easily achievable at low energy.

Another problem that we face in these experiments is the ion background signal. Prior to the interaction with the laser beam, the ion beam is collimated by a 2×2 mm^2 diaphragm. It then enters the interaction region where a static field (typically 10–100 V/cm) is applied. The ion beam is slightly deflected by this static field. Despite all our efforts, a rather large amount of background noise is generated by ions hitting metal surfaces. In order to get rid of a large fraction of this noise, a mass gate is used to reject all masses but the one under study. In addition, after the capture of an experimental image (typically over 5000 laser shots) another image is taken under strictly identical experimental conditions except for the delay between ion extraction and laser firing, which is set out of range. This second image is subtracted from the first one before processing. After subtraction of the background signal, the image is centered and symmetrized. The last step is the inversion of the image, which gives directly a two-dimensional map of the initial velocity. Reference [68] describes the exact inversion procedure relevant to a homogeneous field in the limit of large L/R ratio (L being the length of the spectrometer and R the radius of the detector). As long as the distance between the interaction zone and the detector is large as compared to the radius of the image, R (typically values $L>10$ cm and $R\approx2$ cm fulfill this requirement), this inversion procedure is also relevant to the inhomogeneous field used in velocity map imaging, except for an overall magnification factor easily deduced from calibration measurements. An improved inversion method applicable in any experimental situation is described in Ref. [73].

IV. EXPERIMENTAL RESULTS AND DISCUSSION

A. Images

The smallest system produced with significant abundance in our experiment is the tetramer W_4^-. On the other hand, our limited mass selectivity combined with the presence of numerous isotopes in tungsten and of oxygen impurities prevents the analysis of systems larger than typically $n=15$. Figure 3 presents a typical experimental photoelectron image of W_4^- after absorption of a single photon of energy $h\nu=4.025$ eV ($\lambda=308$ nm). In Fig. 3(a), we present the raw image with background subtraction and symmetrization. The inverted image is presented in Fig. 3(b). The laser polarization is oriented along the vertical axis. The intensity scale

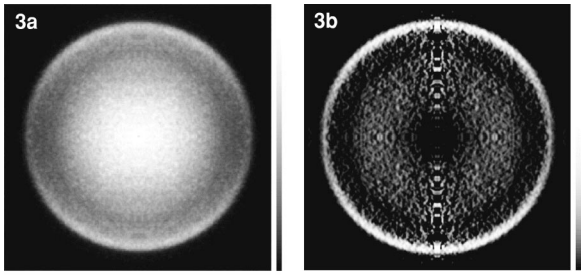

FIG. 3. Typical photoelectron image of W_4^- at $\lambda = 308$ nm. (a) Raw image with background subtraction and symmetrization. The laser polarization is oriented along the vertical axis. The isotropic slow thermal electron distribution is visible in the center of the image. It is surrounded by anisotropic and sharper features corresponding to direct photoemission. (b) Inverted image.

(proportional to electron counts) is represented by a gray scale ranging from black (zero signal) to white (maximum). The images display two main distinct features. A broad distribution is visible in the center of image 3(a), corresponding to slow photoelectrons. This feature is isotropic with respect to the laser polarization. This broad distribution is surrounded by anisotropic (more intense along the laser polarization axis) and sharper features. After inversion [image 3(b)], these two features become, respectively, a broad central ring (secondary peaks along the vertical axis are inversion artifacts) and a larger and sharper ring outside. Remember that the scale of the inverted image is proportional to the electron velocity with $v_e = 0$ in the center. Thus, the width of the central feature when converted to energy is rather small as compared to the outermost structure located at about 2 eV. The shape of the electron distribution near $v_e = 0$ ($\epsilon = 0$) is of primary importance since the observable differences between the various expression for TE are in the range 0–0.5 eV. In particular, the vanishing character of $p(\epsilon)$ at threshold is fundamental. Indeed, in imaging spectroscopy, a nonvanishing distribution at $\epsilon = 0$ will necessarily produce a sharp peak in the center of the image instead of a flat-topped peak as one observes for tungsten cluster anions. Therefore, great care must be taken when recording such images to avoid saturation effects that would artificially smooth any sharp feature in the image.

Experimental raw images for various cluster sizes ($n = 4-11$) are presented in Fig. 4 (with only background subtraction and symmetrization). Both above-mentioned structures are clearly visible in every image: namely, a broad symmetric distribution in the center, surrounded by more or less diffuse ring(s). Regarding the central feature, the most striking point visible in this series of images is that its width decreases progressively as the size of the cluster increases. According to Eq. (12), the width (in energy) of the thermionic emission distribution is proportional to the emission temperature of the cluster, which is itself roughly inversely proportional to the cluster size in the limit of single-photon absorption. The narrowing of the central feature with increasing size, together with its isotropy, is a strong and direct indication that this broad feature is the signature of thermionic emission. Regarding the outer structure, it becomes

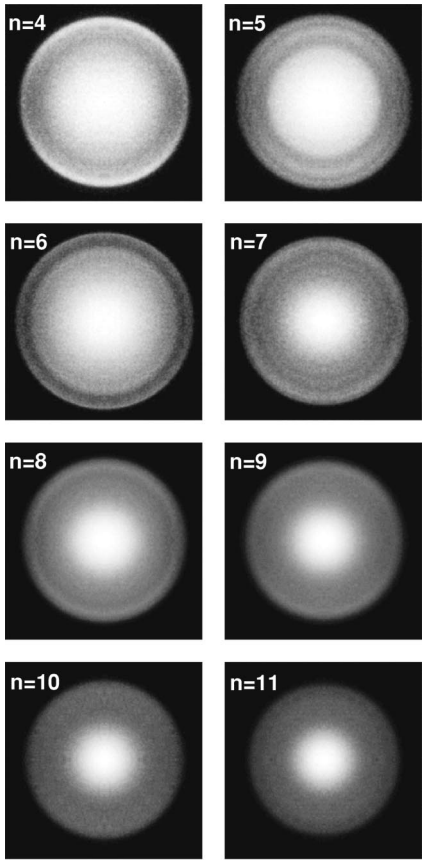

FIG. 4. Raw images for $n = 4-11$.

more and more diffuse and isotropic as the size of the cluster increases. We will discuss this point later.

B. Thermionic emission

After inversion and integration over the angular variable, one obtains the photoelectron kinetic-energy spectra displayed in Fig. 5 ($n = 4-11$). As compared to spectra obtained with more standard techniques such as the magnetic bottle, the resolution of imaging spectroscopy is lower at higher energy. However, its better resolution near threshold allows us to compare our experimental kinetic-energy distributions directly with theoretical predictions. In Fig. 5, distributions calculated in the bulk limit [dashed line, Eq. (3)] and according to Klots' formula [broad solid line, Eq. (12)] are compared with experimental measurements (thin solid line). As discussed in Sec. II, we use as trial value the emission temperature T_e defined by Eq. (7) assuming an initial temperature $T_0 \approx 300$ K. Estimated values of the initial temperature, electron affinity, and emission temperature are given in Table I. In every case, it is assumed that the cluster absorbs a single photon before decaying, which is ensured (at least at small sizes) by working at low laser fluence (typically less than 10 μJ/mm^2 in 20-ns pulses). Refining Eq. (12), one can use the simplest expression for the static polarizability ($\alpha = R_0^3$) in Eqs. (8) and (9) but, in the limit of small-size clusters, this does not make any significant difference and the term proportional to ϵ is completely negligible. The agreement between experimental results and Klots' formula in the

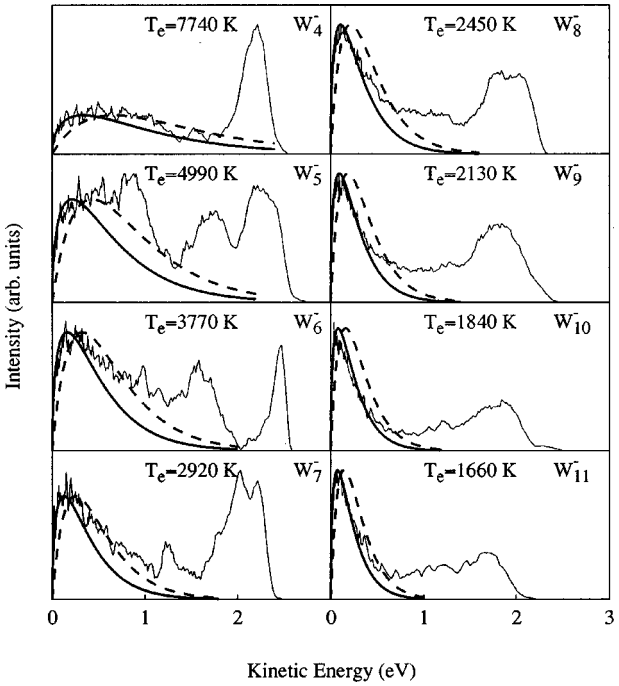

FIG. 5. Photoelectron kinetic-energy spectra obtained after image inversion for W_n^- clusters with $n=4-11$ (thin solid lines). The contribution of thermionic emission [Eq. (12), with the emission temperature T_e given by Eq. (7)], is plotted as the bold solid lines. The dashed lines correspond to the bulk limit [Eq. (3)] at same temperature. Below 0.5 eV, the agreement between experiment and Klots' formula is remarkable. The remaining part of the spectrum is the contribution of direct photoemission.

low-energy range (below 0.5 eV) is excellent and particularly striking at larger sizes ($n>7$). The difference between the bulklike limit expression and Klots' formula is particularly visible here. Indeed (see Fig. 1), for a given emission temperature T_e, the Klots model predicts a maximum in the energy spectrum at $\epsilon_0 \approx k_B T_e/2$ while this maximum is located at $(k_B T_e)$ in the bulk. Hence, there is no ambiguity between the two descriptions and it is clear that the slow-electron distribution observed in the photodetachment of small tungsten cluster anions is essentially due to thermionic emission and is well described by Klots' model.

TABLE I. Internal temperature T_i [Eq. (2)], electron affinity EA (Ref. [34]), estimated emission temperature T_e [Eq. (7)], average fitted temperature $T_{\rm fit}$, and ratio $(T_{\rm fit}/T_e)$ as a function of the cluster size N.

N	T_i (K)	EA (eV)	T_e (K)	$T_{\rm fit}$ (K)	$(T_{\rm fit}/T_e)$
4	9642	1.64	7738	7787	1.006 ± 0.041
5	6138	1.58	4993	5885	1.179 ± 0.226
6	4546	1.48	3766	4414	1.172 ± 0.166
7	3636	1.72	2923	3124	1.069 ± 0.097
8	3048	1.74	2454	2783	1.134 ± 0.040
9	2635	1.73	2134	2198	1.030 ± 0.068
10	2331	1.94	1841	1707	0.927 ± 0.068
11	2096	1.95	1661	1792	1.078 ± 0.088

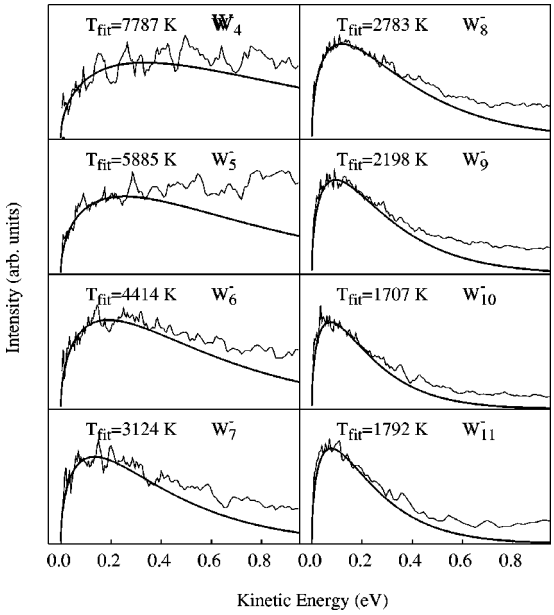

FIG. 6. Enlargement of the photoelectron kinetic-energy spectra between 0.0 and 1.0 eV (thin solid lines). The bold solid lines are the result of a fit of the emission temperature according to Eq. (12).

Kinetic-energy spectra are enlarged between 0.0 and 1.0 eV in Fig. 6. In this figure, experimental spectra are compared with Klots' formula with a temperature $T_{\rm fit}$ fitted to Eq. (12). The fitting procedure is repeated for various energy ranges from 0–0.2 to 0–0.4 eV and an average value of $T_{\rm fit}$ is determined (see Table I). At smaller size, thermionic emission and direct photoemission may overlap and the fitting procedure is not very accurate. This is particularly evident for W_5^-, where a broad structure centered on 0.9 eV is superimposed on thermionic emission. The ratio between fitted temperature and temperature estimated according to Eq. (7) is reported in Table I and plotted in Fig. 7. In any case this ratio is close to 1 and confirms the validity of our assumptions. Note, however, that in general the fitted temperature is

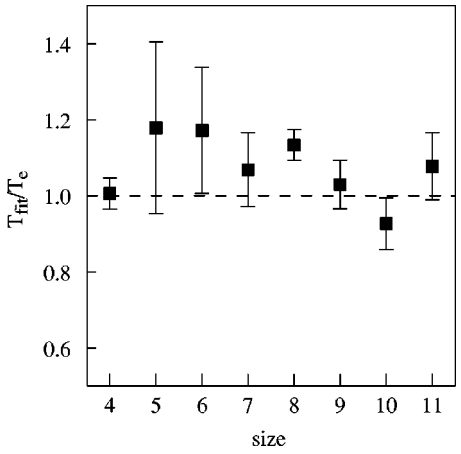

FIG. 7. Ratio between fitted temperature derived from the experimental spectra and temperature estimated according to Eq. (7).

larger than the estimated emission temperature. This slight discrepancy may be due to the presence of a weak two-photon absorption. Considering the crudeness of the various approximations, the agreement is remarkable. Of course, as compared to other methods relying on evaporation measurements [74,75], for instance, the kinetic-energy spectrum in thermionic emission is not a precise thermometer or a precise tool to measure the heat capacity of the clusters. However, it turns out that in this high-temperature regime (2000–7000 K) and at such small size not many other thermometers are available. At this point, one might comment about the very high temperature value reached in smaller systems. In the case of W_4^- and W_5^-, the internal temperature of the cluster is extremely high (respectively, 9600 and 6100 K), well above the vaporization temperature of bulk tungsten. In fact, small extremely hot refractory clusters do not evaporate atoms simply because, despite this extremely high temperature, the internal energy is not sufficient to eject an atom. Indeed, the total internal energy of about 4 eV is too small as compared to the dissociation energy of about 7–8 eV.

The excellent agreement between experiment and model is somewhat surprising at small size ($n=4,5,...$) where the relevance of a thermalization process is questionable. In fact, it is likely that the structureless continuum expected in thermionic emission of a large cluster may be seen as a vibrational progression in small clusters, provided that the experimental resolution is good enough. This kind of vibrational structure is visible, for example, in Si_4^- [76,77]. Owing to the larger mass of tungsten and its more complex electronic structure, it is not visible even in smaller species. Obviously, the building up of the continuum from the vibrational structure (autodetachment) would be more easily observed in lighter elements with larger vibrational constants. From this point of view, understanding the transition from a structured spectrum with intensities governed by electron-ion couplings and Franck-Condon factors to a statistical distribution is a real challenge. Whatever the detailed mechanism of the thermalization, our experimental results strongly support the assumption of an equipartition of the internal energy in small metal clusters.

C. Direct photoemission

Owing to their anisotropic character, the structures observed at higher kinetic energy in the outer part of the image may be attributed without ambiguity to direct photoemission. These structures correspond essentially to the building up of the *d* valence band of tungsten. The outermost ring arises from the transition between the ground state of the anion and the ground state of the neutral species. As is visible in the images (Fig. 4) and the kinetic-energy spectra (Fig. 5), this broad feature is more or less structured depending on the size of the cluster. It is comparatively sharper at $n=4$ and 6, several bands are clearly separated at $n=5$ and 7, while structures are broader at larger sizes. Very few *ab initio* or model calculations are available for W_n^- and W_n clusters [78,79] and none of them allow estimation of the angular distributions that we discuss below.

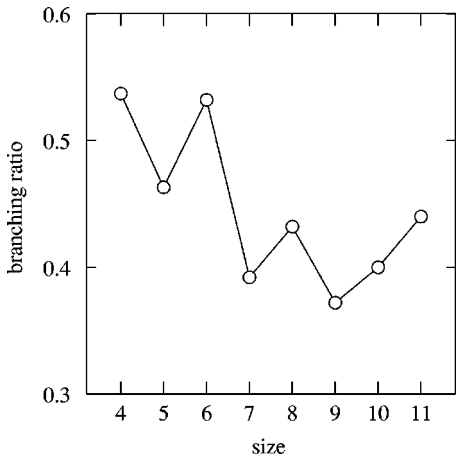

FIG. 8. Branching ratio $\rho_{TE}=I_{TE}/I_{total}$ as a function of cluster size. In the range $n=4-11$, both decay processes are of comparable magnitude ($\rho_{TE}\approx 0.4-0.5$).

In previous work performed on W_n^- clusters [34–37], part of the large difference between the total spectrum and thermionic emission was attributed to inelastic electron scattering. This interpretation was essentially based on the wrong argument that the thermionic emission distribution was simply proportional to $\exp(-\epsilon/k_BT_e)$. Under this assumption, a significant fraction of the continuous spectrum at low energy could not be attributed to thermionic emission and was at the same time not likely to be attributable to direct photoemission. In fact, the correct expression Eq. (12) represents almost all signal at low energy and it seems that no other processes need to be invoked in order to explain the experimental observations. However, electron-electron collisions (inelastic electron scattering) do occur, probably in the initial step of the internal-energy redistribution a few hundreds of femtoseconds after optical excitation. This electron scattering may lead to a thermalization of the conduction electrons before thermalization of all degrees of freedom. Consequently, these hot electrons can in principle be emitted sooner and with a larger kinetic energy than electrons arising from thermionic emission. It is thus possible that such electronic collisions contribute to a fraction of the observed spectrum. However, considering the present results, it is unlikely that a significant proportion of the emitted electrons corresponds to this process evidenced in femtosecond experiments on C_{60} [57]. Only a time-dependent study could distinguish prompt electrons emitted directly after electron-electron collision from delayed electrons ejected after complete thermalization.

We can extract the branching ratio between thermionic (intensity I_{TE}) and total emission (intensity I_{total}) from the experimental data and from a fit to Eq. (12) for the slow photoelectrons. The ratio $\rho_{TE}=I_{TE}/I_{total}$ is plotted in Fig. 8. This ratio is remarkably constant over the whole range studied here ($n=4-11$) and close to 0.4–0.5 as already noted in previous work [34]. This means that both main decay processes (TE and DPE) are of comparable magnitude. This is rather surprising since, at both limits (atom and bulk) ρ_{TE} should vanish. On one hand, direct emission dominates in atoms and dimers where thermionic emission does not exist.

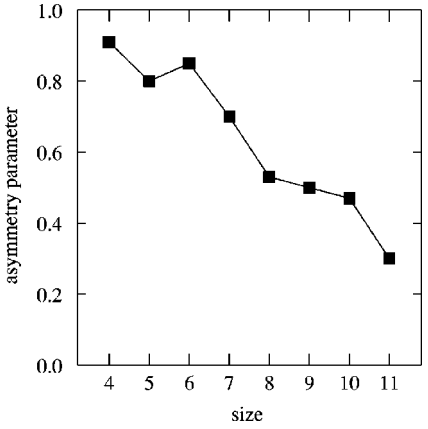

FIG. 9. Asymmetry parameter β of the most intense band observed in direct photoemission as a function of cluster size. The photoemission of small systems is strongly anisotropic and aligned along the laser polarization axis ($\beta \approx 1$). It becomes more isotropic as the size of the system increases ($\beta \rightarrow 0$).

On the other hand, the temperature of a large system does not increase significantly after absorption of a single photon, which precludes thermionic emission. However, in large systems, even though the internal temperature corresponding to the absorption of a single photon is lower, the ratio ρ_{TE} remains about the same, indicating that the increasing number of vibrational degrees of freedom is accompanied by an increase of the electron-phonon coupling.

One of the main advantages of imaging techniques is to provide simultaneously the angular and kinetic-energy distributions. As already mentioned, this capability allows one to discriminate between a direct process, which leads usually to anisotropic distributions, and an indirect process like thermionic emission, which leads to a totally isotropic distribution. More quantitatively, the anisotropy of the photoelectron distribution in a given energy range is measured by the asymmetry parameter β defined as

$$I(\Theta) = (\sigma_T/4\Pi)[1 + \beta P_{20}(\cos\Theta)]. \tag{14}$$

with $-1 \leqslant \beta \leqslant 2$, Θ the angle between the laser polarization axis and the direction of ejection of the electron, and the Legendre polynomial $P_{20}(\cos\Theta) = \frac{3}{2}\cos^2\Theta - \frac{1}{2}$. In Fig. 9 we have plotted the asymmetry parameter β of the most intense band observed in direct photoemission for each cluster size. The general trend in the evolution of this parameter is a monotonic decrease with n. The DPE of small systems is strongly anisotropic and aligned along the laser polarization axis ($\beta \sim 1$). It becomes more isotropic as the size of the system increases ($\beta \rightarrow 0$). The parameter β is closely related to the angular correlations occurring in the photodetachment process. In other words, β depends on the radial and angular properties of the wave functions of the initial and final states of the system. Angular correlations in metal clusters containing a large number of free electrons are extremely difficult to analyze and beyond the scope of the present paper. However, it is very unlikely that a direct photoionization or photodetachment process in a complex system would lead to a totally isotropic emission, as observed in the present case at large N values. Therefore, we may suppose that the observed structures attributed to the building up of the d valence band of tungsten do not strictly correspond to direct photoemission. Rather, the rapid decrease of β with size may be interpreted as an indication of the loss of coherence induced by electron-electron collisions. Therefore, even though electron-electron scattering seems to have no effect on the energy spectrum, it may indirectly influence electron emission.

The asymmetry parameter β is found to be positive for every discrete structure observed in the photodetachment of tungsten cluster anions. This seems to be a general trend in metal clusters as opposed to covalent species such as carbon clusters [80] where this parameter is often negative. While at the moment we have no definitive explanation of this strong qualitative difference, it is not surprising that systems that are correctly described as small metallic spheres behave like a simple dipole with a preferential electron emission along the polarization axis. Indeed, this is a rather general trend in photoionization in the classical picture. The electron emission is preferentially aligned along the laser polarization axis. However, this is less systematic in photodetachment. On the other hand, covalent clusters cannot be modeled by metallic spheres and it is thus not surprising that they exhibit a different behavior. Although we are not able to present any quantitative explanation of the observed measurement of β, it is clear that the evolution of the asymmetry parameter with cluster size contains significant physical information that deserves more refined calculations. Together with the observation of electronic structure, measurement of the asymmetry parameter is a challenge for quantum chemistry of complex systems. At this point, accurate theoretical predictions are absolutely required in order to go further.

D. Decay rate

The last point to discuss is the relatively high thermionic emission rate observed in our experiments. Although we have no direct measurement of these rates, we have some qualitative indications about the lifetime of excited cluster anions with respect to thermionic decay. In the present experiment, the residence time of the clusters in the interaction zone is in the range 0.1–1 μs so that only relatively fast processes are visible. Although not measurable in velocity map imaging, previous observations in standard imaging allow us to give an upper bound for the lifetime of the excited cluster with respect to TE. The asymmetry of the image along the ion beam path provides, in that case, a direct measurement of the lifetime. In every situation presented here, this lifetime is shorter than 100 ns. This time scale for thermionic ''delayed'' emission is extremely short as compared to those obtained, for example, in thermionic emission of neutral tungsten clusters [31–33] or neutral fullerenes [17–30] (usually several microseconds or even milliseconds). However, in the present case, the emission rate, which, in the bulklike limit is determined by Eq. (4), is relatively high owing to the low value of the barrier W to the emission of electrons. For cluster anions, this barrier is simply the electron affinity of the clusters. It is smaller than 2 eV, to be compared with 7–9 eV for the ionization potential of tung-

sten clusters or fullerenes. As a consequence, the exponential term $\exp(-W/k_B T)$ in Eq. (4) is significantly larger (by several orders of magnitude) for anions. This explains the high emission rate and conversely the short lifetime versus thermionic emission for W_n^- clusters. Accurate measurements of these rates under our experimental conditions are not yet available. However, the large discrepancies between measured and predicted rate values reported by other authors are a strong encouragement to perform such absolute measurements. Indeed, our present estimate of the rate (above $10^7\ s^{-1}$) is in contradiction with recent measurements in the Mainz ion trap [36] where lifetimes in the millisecond range have been measured for the same species at comparable excitation energy. This apparent discrepancy may be due to the coexistence of various decay processes and internal bottlenecks leading to different decay paths with completely different time scales. Indeed, our experimental detection time window favors phenomena taking place at short time (less than 1 μs) while experiments in a trap are not sensitive to these fast processes. The fact that the one-photon excitation occurs well above the detachment threshold while, in neutrals, the absorption of several photons is required has, in principle, no direct influence on the internal dynamics of the system. The ''fast'' character of this delayed process is not in contradiction with the long lifetime usually associated with TE and seems to be entirely due to the low electron binding energy. However, it supposes that the internal-conversion rate itself is fast enough to lead to a rapid equilibrium. This means that such systems do not exhibit internal bottlenecks or that current estimations of the various emission rates suffer from wrong assumptions. In any case, further experimental measurements of absolute decay rates together with more detailed theoretical description are required.

V. CONCLUSION

We have shown that thermionic emission is the major slow photoelectron decay channel for refractory cluster anions. Owing to our careful study of the kinetic-energy distribution of threshold electrons, experimental results could be compared with theoretical predictions. In particular, we have shown that the thermal distribution cannot be described by a simple bulklike formula, or by a simple Boltzmann formula. On the contrary, our results are in excellent agreement with the small-metallic-sphere model of Klots [46–53]. Our results indicate that the transition toward a bulklike statistical behavior of the internal-energy redistribution occurs very rapidly, as early as $n=4$, owing to the high density of states in metallic clusters. The observation of the angular distribution of photoelectrons has proved to be a powerful tool to discriminate between direct decay processes and delayed thermionic emission. Note also that the presence of the broad distribution of slow thermal photoelectrons near threshold, whatever the wavelength of the excitation laser, prohibits high-resolution threshold spectroscopy such a zero electron kinetic-energy (ZEKE) anion spectroscopy [81] on such systems.

Besides these results, a number of questions are still open. We have already mentioned that accurate *ab initio* calculations are highly desirable to analyze the observed band structure in direct photoemission and more specifically the angular distribution. However, the main question is concerned with the internal dynamics in such clusters. In particular, what are the detailed mechanisms of the internal-energy redistribution: inelastic electron scattering and electron-phonon couplings? From this point of view, time-resolved experiments could probably allow one to distinguish the two mechanisms since, in principle, they should exhibit specific time scales differing by orders of magnitude. This has recently been performed in very small clusters like, for instance, platinum trimer anions [82]. Another issue is the relevance of defining properly an internal temperature in a system containing only a few atoms. It is clear that only the internal energy has a precise and unquestionable definition. The phase space of a system containing only four atoms is clearly too small to justify entirely a statistical thermodynamic approach. The observation of the building up of this statistical energy redistribution in very small systems by time-resolved photoelectron spectroscopy or ZEKE spectroscopy [83,84] is probably among the most challenging topics in the field of molecular and cluster excited-state dynamics.

ACKNOWLEDGMENTS

Fruitful discussions with Professor Hanspeter Helm are gratefully acknowledged. The ''Laboratoire de Spectrométrie Ionique et Moléculaire'' is a Unité Mixte de Recherche CNRS–Université Lyon I (UMR CNRS 5579).

[1] E. W. Schlag, J. Grotemeyer, and R. D. Levine, Chem. Phys. Lett. **190**, 521 (1992).
[2] F. Remacle and R. D. Levine, Phys. Lett. A **173**, 284 (1993).
[3] F. Remacle and R. D. Levine, Mol. Phys. **87**, 899 (1996).
[4] F. Remacle and R. D. Levine, J. Phys. Chem. A **102**, 10195 (1998).
[5] E. E. B. Campbell and R. D. Levine, Comments Mod. Phys. D **1**, 155 (1999).
[6] H. Weidele, S. Becker, H. J. Kluge, M. Lindinger, L. Schweikhard, C. Walther, J. Ziegler, and D. Kreisle, Surf. Rev. Lett. **3**, 541 (1996).
[7] A. Amrein, R. Simpson, and P. Hackett, J. Chem. Phys. **94**, 4663 (1991).
[8] K. Athanassenas, T. Leisner, U. Frenzel, and D. Kreisle, Ber. Bunsenges. Phys. Chem. **96**, 1192 (1992).
[9] B. D. May, S. F. Cartier, and A. W. Castleman, Jr., Chem. Phys. Lett. **242**, 265 (1995).
[10] S. F. Cartier, B. D. May, and A. W. Castleman, Jr., J. Chem. Phys. **104**, 3423 (1996).
[11] S. E. Kooi and A. W. Castleman, Jr., J. Chem. Phys. **108**, 8864 (1998).
[12] E. E. B. Campbell, G. Ulmer, and I. V. Hertel, Phys. Rev. Lett.

67, 1986 (1991).
[13] A. C. Jones, M. J. Dale, M. R. Banks, I. Gosney, and P. R. R. Langridge-Smith, Mol. Phys. **80**, 583 (1993).
[14] Y. Zhang and M. Stuke, Phys. Rev. Lett. **70**, 3231 (1993).
[15] B. A. Collings, A. H. Amrein, D. M. Rayner, and P. A. Hackett, J. Chem. Phys. **99**, 4174 (1993).
[16] K. Athanassenas, T. Leisner, U. Frenzel, D. Kreisle, and E. Recknagel, Z. Phys. D: At., Mol. Clusters **26**, 153 (1993).
[17] S. Maruyama, M. Y. Lee, R. E. Haufler, Y. Chai, and R. E. Smalley, Z. Phys. D: At., Mol. Clusters **19**, 409 (1991).
[18] P. Sandler, C. Lifshitz, and C. E. Klots, Chem. Phys. Lett. **200**, 445 (1992).
[19] P. Wurz and K. R. Lykke, J. Phys. Chem. **96**, 10129 (1992).
[20] G. Walder and O. Echt, Int. J. Mod. Phys. B **6**, 3881 (1992).
[21] E. E. B. Campbell, G. Ulmer, and I. V. Hertel, Z. Phys. D: At., Mol. Clusters **24**, 81 (1992).
[22] D. Ding, R. N. Compton, R. E. Haufler, and C. E. Klots, J. Phys. Chem. **97**, 2500 (1993).
[23] G. Walder, K. W. Kennedy, and O. Echt, Z. Phys. D: At., Mol. Clusters **26**, 288 (1993).
[24] C. Yeretzian, K. Hansen, and R. L. Whetten, Science **260**, 652 (1993).
[25] D. Ding, J. Huang, R. N. Compton, C. E. Klots, and R. E. Haufler, Phys. Rev. Lett. **73**, 1084 (1994).
[26] C. E. Klots, R. N. Compton, M. Stuke, and Y. Zhang, Phys. Rev. Lett. **76**, 4092 (1996).
[27] K. Hansen and O. Echt, Phys. Rev. Lett. **78**, 2337 (1997).
[28] Rongping Deng and O. Echt, J. Phys. Chem. A **102**, 2533 (1998).
[29] G. von Helden, I. Holleman, A. J. A. van Roij, G. M. I. Knippels, A. F. G. van der Meer, and G. Meijer, Phys. Rev. Lett. **81**, 1825 (1998).
[30] A. Bekkerman, B. Tsipinyuk, A. Budrevich, and E. Kolodney, J. Chem. Phys. **108**, 5165 (1998).
[31] A. Amrein, R. Simpson, and P. Hackett, J. Chem. Phys. **95**, 1781 (1991).
[32] T. Leisner, K. Athanassenas, O. Echt, O. Kandler, D. Kreisle, and E. Recknagel, Z. Phys. D: At., Mol. Clusters **20**, 127 (1991).
[33] T. Leisner, K. Athanassenas, D. Kreisle, E. Recknagel, and O. Echt, J. Chem. Phys. **99**, 9670 (1993).
[34] H. Weidele, D. Kreisle, E. Recknagel, G. S. Icking-Konert, H. Handschuh, G. Ganteför, and W. Eberhardt, Chem. Phys. Lett. **237**, 425 (1995).
[35] G. Ganteför, W. Eberhardt, H. Weidele, D. Kreisle, and E. Recknagel, Phys. Rev. Lett. **77**, 4524 (1996).
[36] H. Weidele, D. Kreisle, E. Recknagel, S. Becker, H. J. Kluge, M. Lindinger, D. L. Schweikhard, C. Walther, and J. Ziegler, J. Chem. Phys. **110**, 8754 (1999).
[37] G. H. Lee, S. H. Huh, Y. C. Park, F. Hayakawa, Y. Negishi, A. Nakajima, and K. Kaya, Chem. Phys. Lett. **299**, 309 (1999).
[38] J. C. Pinaré, B. Baguenard, C. Bordas, and M. Broyer, Phys. Rev. Lett. **81**, 2225 (1998).
[39] J. C. Pinaré, B. Baguenard, C. Bordas, and M. Broyer, Eur. Phys. J. D **9**, 21 (1999).
[40] Lai-Sheng-Wang, J. Conceicao, J. Changming, and R. E. Smalley, Chem. Phys. Lett. **182**, 5 (1991).
[41] P. Hvelplund, Phys. Scr., T **T59**, 244 (1995).
[42] K. Hansen, J. U. Andersen, H. Cederquist, C. Gottrup, P. Hvelplund, M. O. Larsson, V. V. Petrunin, and H. T. Schmidt, Eur. Phys. J. D **9**, 351 (1999).
[43] N. W. Ashcroft and N. D. Mermin, *Solid State Physics* (Saunders, London, 1976).
[44] G. von Helden, I. Holleman, G. M. H. Knippels, A. F. G. van der Meer, and G. Meijer, Phys. Rev. Lett. **79**, 5234 (1997).
[45] G. von Helden, I. Holleman, M. Putter, A. J. A. van Roij, and G. Meijer, Chem. Phys. Lett. **299**, 171 (1999).
[46] C. E. Klots, J. Chem. Phys. **90**, 4470 (1989).
[47] C. E. Klots, J. Chem. Phys. **93**, 2513 (1990).
[48] C. E. Klots, J. Chem. Phys. **93**, 6585 (1990).
[49] C. E. Klots, Chem. Phys. Lett. **186**, 73 (1991).
[50] C. E. Klots, Z. Phys. D: At., Mol. Clusters **20**, 105 (1991).
[51] C. E. Klots, J. Chem. Phys. **98**, 1110 (1993).
[52] C. E. Klots, J. Chem. Phys. **100**, 1035 (1994).
[53] C. E. Klots and R. N. Compton, Surf. Rev. Lett. **3**, 535 (1996).
[54] D. H. Parker and A. T. J. B. Eppink, J. Chem. Phys. **107**, 2357 (1997).
[55] A. T. J. B. Eppink and D. H. Parker, Rev. Sci. Instrum. **68**, 3477 (1997).
[56] C. Voisin, D. Christofilos, N. Del Fatti, F. Vallée, B. Prével, E. Cottancin, J. Lermé, M. Pellarin, and M. Broyer, Phys. Rev. Lett. **85**, 2200 (2000).
[57] E. E. B. Campbell, K. Hansen, K. Hoffmann, G. Korn, M. Tchaplyguine, M. Wittmann, and I. V. Hertel, Phys. Rev. Lett. **84**, 2128 (2000).
[58] J. U. Andersen, C. Brink, P. Hvelplund, M. O. Larsson, B. Bech-Nielsen, and H. Shen, Phys. Rev. Lett. **77**, 3991 (1996).
[59] U. Frenzel, U. Hammer, H. Westje, and D. Kreisle, Z. Phys. D: At., Mol. Clusters **40**, 108 (1997).
[60] W. A. Chupka and C. E. Klots, Int. J. Mass Spectrom. Ion Processes **167-168**, 595 (1997).
[61] K. Hansen and E. E. B. Campbell, Phys. Rev. E **58**, 5477 (1998).
[62] C. E. Klots, J. Chem. Phys. **83**, 5854 (1985).
[63] C. E. Klots, Z. Phys. D: At., Mol. Clusters **5**, 83 (1987).
[64] C. E. Klots, Nature (London) **327**, 222 (1987).
[65] C. E. Klots, Phys. Rev. A **39**, 339 (1989).
[66] H. Helm, N. Bjerre, M. Dyer, D. Huestis, and M. Saeed, Phys. Rev. Lett. **70**, 3221 (1993).
[67] C. Bordas, M. J. Dyer, T. Fairfield, H. Helm, and K. C. Kulander, Phys. Rev. A **51**, 3726 (1995).
[68] C. Bordas, F. Paulig, H. Helm, and D. L. Huestis, Rev. Sci. Instrum. **67**, 2257 (1996).
[69] J. U. Andersen, E. Bonderup, and K. Hansen (unpublished).
[70] W. A. de Heer, Rev. Mod. Phys. **65**, 611 (1993).
[71] P. Milani and W. A. de Heer, Rev. Sci. Instrum. **61**, 1835 (1990).
[72] P. Kruit and F. H. Read, J. Phys. E **16**, 313 (1983).
[73] J. Winterhalter, D. Maier, J. Honerkamp, V. Schyja, and H. Helm, J. Chem. Phys. **110**, 11 187 (1999).
[74] M. Schmidt, R. Kusche, W. Kronmüller, B. von Issendorf, and H. Haberland, Phys. Rev. Lett. **79**, 99 (1997).
[75] R. Kusche, Th. Hippler, M. Schmidt, B. von Issendorf, and H. Haberland, Eur. Phys. J. D **9**, 1 (1999).
[76] C. C. Arnold and D. M. Neumark, J. Chem. Phys. **99**, 3353 (1993).
[77] C. C. Arnold and D. Neumark, Adv. Met. Semicond. Clusters **3**, 113 (1995).

[78] G. Seifert, E. Mrosan, and H. Muller, Phys. Status Solidi B **89**, 553 (1978).
[79] K. Balasubramanian and D. Dingguo, Chem. Phys. Lett. **265**, 538 (1997).
[80] B. Baguenard, J. C. Pinaré, F. Lépine, C. Bordas, and M. Broyer (unpublished).
[81] C. Bäßmann, U. Boesl, D. Yang, G. Drechsler, and E. W. Schlag, Int. J. Mass Spectrom. Ion Processes **159**, 153 (1996).
[82] N. Pontius, P. S. Bechthold, M. Neeb, and W. Eberhardt, Phys. Rev. Lett. **84**, 1132 (2000).
[83] E. W. Schlag, *Zeke Spectroscopy* (Cambridge University Press, Cambridge, 1998).
[84] K. Müller-Dethlefs and E. W. Schlag, Annu. Rev. Phys. Chem. **42**, 109 (1991).